ELSEVIER

Thermochimica Acta 307 (1997) 185–195

thermochimica acta

# Thermal effect on BaFCl: High-temperature X-ray diffraction

R. Kesavamoorthy*, B. Sundarakkannan, G.V. Narasimha Rao, V. Sankara Sastry

*Materials Science Division, Indira Gandhi Centre for Atomic Research, Kalpakkam 603 102, India*

Received 16 June 1997; received in revised form 17 October 1997; accepted 24 October 1997

**Abstract**

Results of the Rietveld analysis of high-temperature powder XRD data of BaFCl are reported and discussed for the first time. The values of $a$ and $c$ increase monotonically with $T$ while those of $c/a$ and density decrease. Linear thermal expansion coefficients pass through a minimum at ca. 350°C. The cell parameters depend on the sample preparation conditions. The interplanar separation distance between Ba and F planes decreases while that between Ba and $Cl_1$ planes, and between $Cl_1$ and $Cl_2$ planes, increases with temperature. The bond length, connecting any ion with Ba, and that between $Cl_1$ and $Cl_2$ increases with $T$. The sintering of the sample powder is manifested in many of the Rietveld parameters. The efficiency of the Rietveld analysis of powder XRD data in obtaining the cell parameters, fractional coordinates, sample compaction, preferred orientation, etc. has been amply demonstrated. © 1997 Elsevier Science B.V.

*Keywords:* BaFCl; EGA; HTXRD; Rietveld analysis; Thermal expansion

## 1. Introduction

Ternary PbFCl-type compounds MFX (M: Ca, Sr, Ba; X: Cl, Br, I) are promising phosphor host crystals. Single crystals of MFX are grown by the flux method [1], the Bridgman method [2] and the modified Kyropoulos method [3]. MFX crystallizes in tetragonal P4/nmm ($D_{4h}^7$) symmetry with a platelet morphology. Cleavage is perpendicular to the $c$-axis, wfhere bonding between the neighbouring $x$-planes is weaker [4]. The growth rate in the basal plane is at least twenty times greater than along the $c$-axis [3]. It is reported that thick single crystals of MFX can be obtained in horizontal Bridgman growth by mixing $MF_2$ and $MX_2$ in a stoichiometrically $F$-rich proportion [5]. In the modified Kyropoulos method, thicker crystals can be grown using a ring heater around the growth interface, but they tend to have a lot of inclusions [3]. The flux method yields high quality single crystals having relatively low thickness. However, dendritic growth was observed in such crystals [1,6].

MFX crystals have been investigated extensively. High-pressure X-ray diffraction on MFX reveals a structural phase transition [7]. However, the high-pressure phase has not yet been identified. Raman and infrared modes in these crystals have been reported [6,8,9]. A high-temperature Raman study has not indicated any structural phase transitions from 25° to 700°C [10]. The mode frequencies have been calculated and compared with the experimental values [11,12]. Extensive lattice-dynamics calculations have been carried out to obtain phonon dispersion relations, elastic constants, phonon density of states and specific

*Corresponding author. Tel.: 00 91 04114 40381; fax: 00 91 04114 40396; e-mail: rkm@igcar.ernet.in


*PII* S0040-6031(97)00414-0

heats of these crystals [12–14]. Ultrasonic and Brillouin scattering measurements in these crystals [15] and cohesive energy calculations [16] confirm the predominantly ionic nature of the bonds, which is a basic input to the phonon calculations [12–14]. Single crystal X-ray diffraction from BaFCl has been carried out at room temperature [3,4] and at elevated temperatures, from 25° to 610°C [17]. These investigations provide lattice parameters [3], fractional coordinates of the ions and the anisotropic thermal parameters of BaFCl [4]. Kodama et al. [17] have determined the anharmonic potential parameters up to the third order using their high-temperature (HT) XRD data on BaFCl single crystal.

When MFX crystals are doped with rare earths like Eu, Sm, etc., they show luminescence and photostimulated luminescence [5]. Emerging filmless radiography techniques take advantage of photostimulated luminescence and replace the X-ray films with phosphor plates made of BaFBr : $Eu^{2+}$ [5]. BaFCl : $Sm^{2+}$ has been proposed to be a replacement for ruby as pressure calibrant in diamond anvil cell technique [2]. These phosphors, MFX doped with rare earths, are used as the sensors for X-ray, gamma ray, electrons, positrons and neutrons. Investigations on the defect-centre generation and their properties in MFX have been carried out extensively [18–21]. Presently, colour-centre lasers using alkali-earth dihalides (MFX) are being developed.

In spite of their tremendous potential in various applications, thermal data on MFX are scanty. In this work, the powder XRD patterns of BaFCl, grown by the flux method, is reported from 25° to 600°C. XRD [3,4] and HTXRD [17] data were reported for the BaFCl single crystals. The powder XRD data on BaFCl at room temperature have been taken previously [ICDD pattern No. 240096], but not at elevated temperatures. Also, these patterns were not analysed using the Rietveld program. The present powder XRD patterns are analysed using the Rietveld program [22–24] for the first time. The $a$ and $c$ lattice parameters, and the fractional coordinates of the Ba ion ($Z_{Ba}$) and that of the Cl ion ($Z_{Cl}$) in the unit cell are obtained. The linear thermal expansion coefficients $\alpha_{\|}$ and $\alpha_{\perp}$, density, $c/a$ ratio, line shape function, full width at half maximum (FWHM) and the asymmetry of XRD peaks are reported and explained. The sample powder is found to sinter during the high-temperature XRD experiment. No structural phase transition has been observed in this temperature range, which is in agreement with the high-temperature Raman data [10] as well as with the HTXRD single-crystal data [17]. The interplanar separation distances between the adjacent planes of F and Ba, Ba and $Cl_1$, and $Cl_1$ and $Cl_2$ as well as the interionic distances between F and Ba, Ba and $Cl_1$, Ba and $Cl_2$, and $Cl_1$ and $Cl_2$ are reported. BaFCl powder was heated to 950°C in a helium atmosphere and then allowed to cool to room temperature. The XRD pattern of the heat-treated BaFCl shows that the lattice parameters have decreased due to heat treatment. F and Cl evolve at high temperatures from BaFCl. The results are discussed.

## 2. Experimental

Clear, transparent and dendrite-free single crystals of BaFCl ($5\times5\times0.5$ mm$^3$) were grown by the flux method. To grow single crystals of BaFCl, the powders of $BaCl_2{\cdot}2H_2O$ and KF (both LOBA GR grade) were mixed in an equal mole fraction and ground thoroughly in a mortar and pestle. The XRD pattern of the mixture showed the presence of BaFCl and KCl, indicating that reaction occurred during grinding. This mixed powder was loaded into a platinum crucible and placed in a vertical canthal-wound muffle furnace at 600°C. It was heated to 860°C and kept for 2 h to obtain a homogenous solution. The solution was cooled at a rate of 20°C h$^{-1}$ to 700°C and then furnace cooled to room temperature (25°C). The resulting mass contained a lot of BaFCl single crystals embedded in a KCl matrix. Methanol was used to separate the single crystals. Optical microscopic examination before and after etching with conc. $HNO_3$ revealed that the crystals were clear, transparent and dendrite-free. The Laue pattern of the single crystal of BaFCl recorded at room temperature with the $c$-axis parallel to the unfiltered Cu radiation X-ray beam in a Laue camera (Huber Type 802) indicated strain-free single crystal nature. These single crystals were powdered thoroughly for HTXRD measurements. The powder obtained from the single crystals would ensure the purity of the sample. Powder HTXRD patterns were recorded in a SIEMENS D-500 powder diffractometer equipped with HT attachment (HT X-ray chamber, model HDK 2.3, Edmond

Buehler). A tantalum metal foil served as both, the heater and sample holder in this HT attachment. The sample was heated in this attachment at $10^{-5}$ torr vacuum. The temperature was controlled by a programmable temperature controller (Eurotherm, type 818) to within ±0.5°C. A W–Re thermocouple was spot-welded to the rear side of the Ta foil. The sample powder was packed lightly in a 5 mm diameter, 0.5 mm deep depression in the Ta foil. The top surface of the sample powder was in-plane with the Ta foil surface at room temperature. This surface was aligned accurately with the diffractometer axis. The powder XRD data was recorded using Cu$K_\alpha$ radiation. Data were collected in step-scanning mode with a step of $2\theta$=0.05° and dwell time of 10 s at each step between 11° and 43°. XRD peaks of the Ta foil appear in the $2\theta$ range from ca. 35° to 40°. In the present report, the HTXRD data from 11° to 33° were used to determine the lattice parameters and the fractional coordinates.

The BaFCl powder was heated in a flowing helium atmosphere at 10°C $min^{-1}$ to 950°C and then cooled at the same rate to room temperature. The room temperature powder XRD of the pristine and the heat-treated BaFCl were recorded for $2\theta$ in the 5–150° range, in the same powder diffractometer using a different sample holder. The sample was loaded in a 100 μm deep cavity of 6 mm dia, made in a Si(911) wafer.

Evolved gas curves for F, $F_2$, Cl and $Cl_2$ were obtained in a real-time multiple-ion detection trend analysis mass spectrometer [25]. The all-metal ultra-high vacuum chamber was pumped by a turbomolecular pumping system (TSU 330, Blazers, Germany) and a triode sputter ion pump (IZ 270, Leybold-Hereaus, Germany). A quadrupole mass spectrometer (Dataquad, Spectromass, UK) was employed. The UHV chamber was coupled to high-temperature high-vacuum compatible quartz chamber by a variable conductance molecular leak valve (MD7, VG Micromass, UK).

## 3. Rietveld analysis

Lattice parameters, fractional coordinates of the ions in a unit cell and thermal vibration of the ions are usually obtained from single-crystal diffractometry. However, this information could also be retrieved from the powder XRD data. The Rietveld method [22] of structural refinement from powder diffraction patterns is widely used with neutron data and, increasingly, with X-ray data. Many versions of this method of analysing powder XRD data have been reported [23]. In the present work, a version called DBWS-9411 is used [24]. This computer program is designed to carry out Rietveld refinements with X-ray or neutron powder diffraction data in a digitized form collected under any of the most commonly used instrumental conditions, with a restriction that the data must be at equal $2\theta$ intervals.

## 4. Results and discussion

Fig. 1 shows the recorded powder XRD pattern of BaFCl at 25°, 300° and 600°C. It shows five distinct

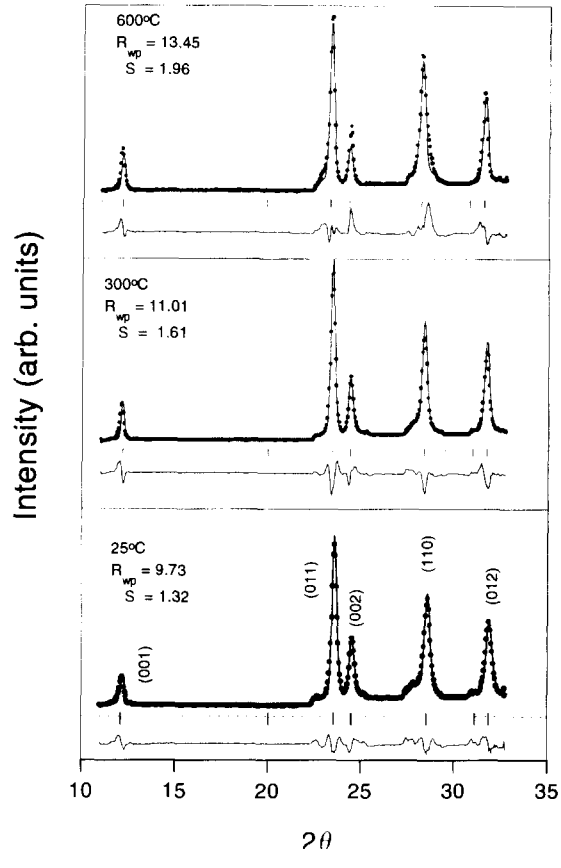


Fig. 1. Rietveld refinement plot of BaFCl at 25°, 300° and 600°C. The points are the powder XRD data. The reflection plane indices are marked. The $2\theta$ values of the calculated diffraction peaks are marked. Residuals are shown in the bottom of each plot.

Table 1
The cell parameters, fractional coordinates of Ba ($Z_{Ba}$), $Cl_I$ ($Z_{Cl}$) and $S$ factor for BaFCl obtained from Rietveld analysis

| $T$/ °C | $a$/ Å | $c$/ Å | $Z_{Ba}$ | $Z_{Cl}$ | $S$ |
|---|---|---|---|---|---|
| 25 | 4.3971(1) | 7.2304(1) | 0.2107(5) | 0.358(2) | 1.32 |
| 100 | 4.4084(1) | 7.2452(1) | 0.2099(6) | 0.358(3) | 1.38 |
| 200 | 4.4226(1) | 7.2644(1) | 0.2084(5) | 0.358(3) | 1.58 |
| 300 | 4.4376(1) | 7.2798(1) | 0.2071(6) | 0.358(3) | 1.61 |
| 400 | 4.4468(1) | 7.2894(1) | 0.2064(6) | 0.356(3) | 1.63 |
| 500 | 4.4593(1) | 7.3032(1) | 0.2053(6) | 0.359(3) | 1.68 |
| 600 | 4.4729(1) | 7.3219(2) | 0.202(1) | 0.356(4) | 1.96 |

diffraction peaks in the $2\theta$ range from 11° to 33°. The plane indices are marked near the corresponding diffraction peaks. Tantalum diffraction peaks interfere with those of BaFCl at $2\theta$ greater than 33° and, hence, the data for higher angles are not presented. The allowed peak positions for the P4/nmm symmetry with BaFCl lattice parameters are marked in this figure. The continuous line through the data points is the fitted line obtained from the Rietveld program. Convergence was achieved quickly using a block approach wherein we adjusted a few parameters while fixing a few other parameters and then the second set of parameters were allowed to vary while the parameters in the first set remained fixed. The first set of parameters was the zero shift, the sample displacement, the scale factor, overall thermal parameter, the width parameters, the preferred orientation, asymmetry and the line shape parameter. The second set of parameters was the $a$ and $c$ lattice parameters and the fractional coordinates of Ba and $Cl_I$ ions along $c$-axis with respect to that of F ion, namely, $Z_{Ba}$ and $Z_{Cl}$. At first, approximate values of the second set of parameters were given. They were fixed and the first set of parameters were adjusted. $R_{wp}$ (the weighted $R$-factor) and $S$ (goodness of fit) were monitored to judge the convergence and the goodness of fit. After the convergence, zero shift, sample displacement, scale factor and overall thermal parameter were fixed and the other parameters along with the lattice parameters and fractional coordinates were adjusted. The values of $R_{wp}$ and $S$ decreased further and converged [24]. Fig. 1 also gives the difference between the experimental XRD data points and the fit. The values of $R_{wp}$ and $S$ increase with increasing temperature, since the data points are increasingly noisy with temperature. Table 1 gives the values of $a$, $c$, $Z_{Ba}$, $Z_{Cl}$ and $S$ at various temperatures as obtained from the Rietveld analysis.

For the sake of checking the convergence in the Rietveld analysis in the event of varying all the 14 parameters simultaneously, the HTXRD data of BaFCl have been analysed by varying both sets of parameters (14 in number) together. It is observed that convergence could be achieved for the XRD data taken from room temperature to 400°C, even if all these 14 refinable parameters were allowed to vary simultaneously. However, the fit did not converge for the data of 500° and 600°C, if all the 14 parameters are varied together. The zero shift, sample displacement, lattice parameters and fractional coordinates were highly correlated. The convergence was not achieved, probably due to the collected data at 500° and 600°C being noisy. Therefore, the block approach of achieving convergence in the Rietveld analysis has been followed at all temperatures from 25° to 600°C.

Interesting results were derived from the fitted parameters of the Rietveld analysis. Fig. 2(a) shows the lattice parameters $a$ and $c$ at various temperatures. Nearly 1.5% change in the lattice parameters is observed over a range of 600°C. The precision in these parameters is ca. 0.002%. The solid lines are the least-squares fitted third-order polynomials through these points. These polynomials are [26]

$$a = \sum_{i=1}^{4} a_i T^{4-i} \tag{1}$$

and

$$c = \sum_{i=1}^{4} c_i T^{4-i} \tag{2}$$

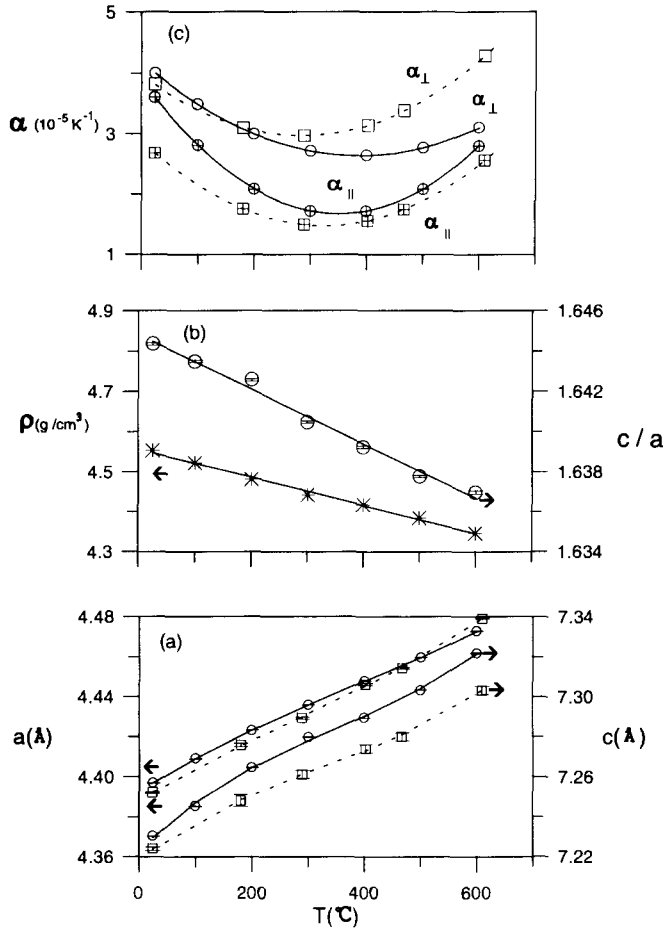


Fig. 2. The temperature dependence of (a) the lattice parameters, (b) density and *c/a* ratio, and (c) linear thermal expansion coefficients. The lattice parameters are fitted to cubic polynomials. The solid straight lines through density and *c/a* ratio are guide to the eye. $\alpha_{\parallel}$ and $\alpha_{\perp}$ are fitted to quadratic polynomials. The solid lines are drawn through the present data (○, ⊕) and the dashed lines are through the reported data of Kodama et al. [17] (□, ⊞).

where $T$ is the temperature (in °C), $a_1=1.5293\times10^{-10}$ Å $K^{-3}$, $a_2=-1.7537\times10^{-7}$ Å $K^{-2}$, $a_3=1.8430\times10^{-4}$ Å $K^{-1}$, $a_4=4.3922$ Å, $c_1=4.4257\times10^{-10}$ Å $K^{-3}$, $c_2=-4.6297\times10^{-7}$ Å $K^{-2}$, $c_3=2.8306\times10^{-4}$ Å $K^{-1}$ and $c_4=7.2227$ Å. Fig. 2(a) also contains the data of Kodama et al. [17]. Their values of $a$(=4.3920(4)) and $c$(=7.224(1)) are slightly lower than our values. The dashed lines are the fit through their data.

The temperature variations of *c/a* and the density are given in Fig. 2(b). The solid straight lines are guide to the eye. The errors in *c/a* and the density are ca. 0.003 and 0.005%, respectively. The density decreases ca. 4.5% in this temperature range almost linearly. The *c/a* ratio decreases from 1.643 to 1.637 as $T$ increases from 25° to 600°C. This behaviour of *c/a* with temperature is interesting when compared with that of pressure. Shen et al. [7] have investigated the effect of high pressure on BaFCl. They have reported that the *a* and *c* lattice parameters as well as *c/a* decrease with the increase of pressure. Both, the increasing pressure and decreasing temperature cause the lattice to shrink. The behaviour of *a* and *c* was consistent with this. But the *c/a* ratio decreases with increasing pressure as well as increasing temperature. When *c/a* reached 1.58, due to the faster decrease of

$c$ as compared to that of $a$, a pressure-induced phase transition occurred in BaFCl at 21 GPa [7]. Here, the $c/a$ ratio reaches only 1.637 at 600°C due to the slower increase of $c$ as compared to that of $a$ and the sample retains the P4/nmm symmetry.

Fig. 2(c) shows the linear thermal expansion coefficient along $c$-axis ($\alpha_{\|}$) and that along $a$ or $b$ axis ($\alpha_{\perp}$). They are obtained from differentiating Eqs. (1) and (2) with respect to the temperature as given by [26]

$$\alpha_{\perp} = \frac{1}{a}\frac{da}{dT} \tag{3}$$

and

$$\alpha_{\|} = \frac{1}{c}\frac{dc}{dT} \tag{4}$$

The values of ($\alpha_{\|}$) and ($\alpha_{\perp}$) obtained using Eqs. (3) and (4) are marked as points. The error in ($\alpha_{\|}$) and ($\alpha_{\perp}$) is ca. 0.2%. The solid lines are the least-squares fitted quadratic polynomials [26],

$$\alpha_{\perp} = \sum_{i=1}^{3} A_i T^{3-i} \tag{5}$$

and

$$\alpha_{\|} = \sum_{i=1}^{3} C_i T^{3-i} \tag{6}$$

where $A_1 = 1.0411 \times 10^{-10}\,K^{-3}$, $A_2 = -8.0477 \times 10^{-8}\,K^{-2}$, $A_3 = 4.1911 \times 10^{-5}\,K^{-1}$, $C_1 = 1.8291 \times 10^{-10}\,K^{-3}$, $C_2 = -1.2813 \times 10^{-7}\,K^{-2}$ and $C_3 = 3.9123 \times 10^{-5}\,K^{-1}$. It is interesting to note that $\alpha_{\|}$ and $\alpha_{\perp}$ are of the order of $3 \times 10^{-5}\,K^{-1}$ and pass through a minimum at ca. 350°C. The increased linear thermal expansion after ca. 350°C in BaFCl could be due to the onset of a new mechanism for the thermal expansion related to the anharmonicity in the Ba and Cl vibrations. A similar temperature dependence of $\alpha_{\|}$ and $\alpha_{\perp}$ in tetramethylammonium halide has been reported [27]; both $\alpha_{\|}$ and $\alpha_{\perp}$ pass through a minimum at ca. 150°C.

Kodama et al. [17] have reported the values of cell parameters and fractional coordinates at various temperatures as determined from their HTXRD data on a BaFCl single crystal. However, they have not analysed their data for $\alpha_{\|}$ and $\alpha_{\perp}$. In the present work, their data have been analysed in the same way as that for the present data and the results are presented in Fig. 2. Interestingly, their data on the cell parameters also show a change of curvature (dashed line) around 350°C as seen in Fig. 2(a). The values of $\alpha_{\|}$ and $\alpha_{\perp}$ (dashed line) also go through a minimum at ca. 350°C as shown in Fig. 2(c). Our values of $a$, $c$, $\alpha_{\|}$ and $\alpha_{\perp}$ are slightly different from theirs [17]. They have used HTXRD data up to $2\theta = 54°$, whereas our powder HTXRD is in a more restricted range of $2\theta$. To ensure that the restricted $2\theta$ range does not unduly affect our results and conclusions, we recorded the powder XRD data of BaFCl at room temperature (25°C) in a wider $2\theta$ range of 5–150° using a different sample holder. The sample was loaded into a 6 mm dia 100 μm deep cavity made in a 1 mm thick Si(911) wafer which served as a low background sample holder plate. Fig. 3(a) shows the powder XRD pattern of pristine BaFCl in the $2\theta$ range of 5–70°, even though it has been recorded up to 150°. The Rietveld analysis of these data up to 150° gave the values of $a$ as 4.3970(1) and that of $c$ as 7.2305(1). On comparing these values of $a$ and $c$ with those obtained from the Rietveld analysis of the RTXRD data of BaFCl powder from 11–33° using tantalum foil as a sample holder (Table 1), we can conclude that the values of $a$ and $c$ obtained from analysis of data in a smaller $2\theta$ range are quite reliable and self-consistent. The lower values of $a$ and $c$ for the samples of Kodama et al. [17] and Sauvage [4] samples as compared to the present sample might be due to the different thermal history seen by the sample during preparation. The flux-grown crystals nucleated from the high-temperature solution at ~835°C on cooling, whereas BaFCl crystals used in the previous studies [4,17] were obtained from BaFCl melt by the Bridgman method, which implies nucleation at ~1008°C and subsequent cooling. This subsequent cooling rate might be different in the samples used by Kodama et al. [17] and Sauvage [4]. To check that the different thermal history could lead to a change in the lattice parameters, we have heated our BaFCl powder in a helium atmosphere from room temperature to 950°C at the rate of 10°C $min^{-1}$ and then cooled it back to room temperature. The room-temperature powder XRD data was recorded on this heat-treated sample in the $2\theta$ range of 5–150° using the Si(911) low-background sample holder. Fig. 3(b) shows this XRD pattern from 5–70°.

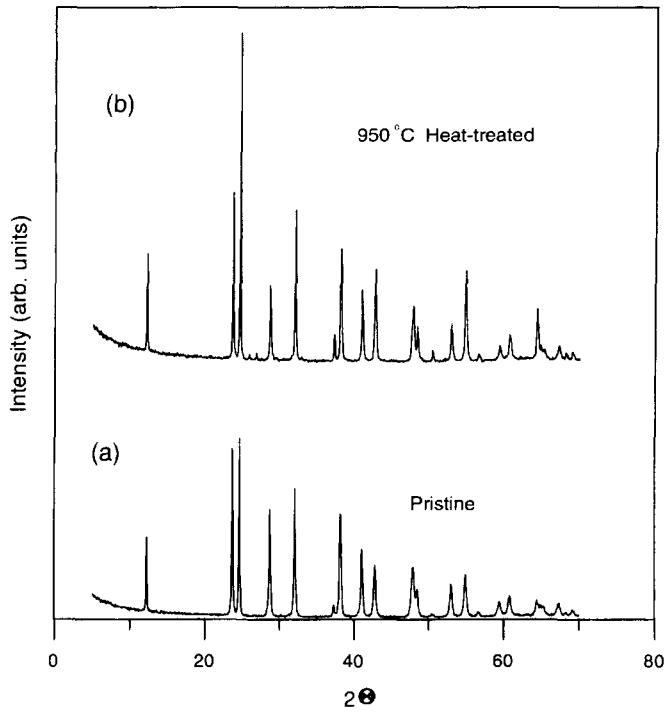


Fig. 3. Powder RTXRD patterns of (a) pristine (b) 950°C heat-treated BaFCl.

The data up to 150° $2\theta$ was analysed using the Rietveld method and the lattice parameter values obtained were $a$=4.3939(1) Å and $c$=7.2257(1) Å. It is thus interesting to note that the cell has shrunk upon heat treatment and the cell parameters are now in excellent agreement with those of Sauvage [4] ($a$=4.3939(6) and $c$=7.2248(9)) and much closer to those of Kodama et al. [17] ($a$=4.3920(4) and $c$=7.224(1)). The XRD pattern recorded using a Si(911) grooved plate shows a large preferred orientation while that recorded using the Ta foil show less preferred orientation. The Rietveld analysis indicates that the preferred orientation factor for the XRD on Ta foil (Fig. 1) is 0.9, that for the pristine sample in a Si(911) wafer (Fig. 3(a)) is 0.8 and for the heat-treated sample in a Si(911) wafer (Fig. 3(b)) is 0.64. The larger the factor, the smaller is the preferred orientation.

Fig. 4 shows the evolved gas curves for F, $F_2$, Cl and $Cl_2$ from BaFCl on heating at 10°C $min^{-1}$. $F_2$ and $Cl_2$ are almost constant in temperature at the background value indicating that they do not evolve from the sample. Chlorine shows a little evolution in the $1–2\times10^{-11}$ torr range, while fluorine shows the evolution from $6–8\times10^{-11}$ torr. The evolution of F and Cl creates F and Cl vacancies in BaFCl. On cooling, the vacancies continued to exist since the evolved gas was pumped out during heating. These vacancies result in the shrinkage of the unit cell which has been observed by the RTXRD of the heat-treated BaFCl.

Fig. 5 illustrates the ionic positions in the BaFCl unit cell. Planes containing all F ions, Ba ions, $Cl_1$ ions, $Cl_2$ ions, Ba ions and F ions are stacked one over the other along the $c$-axis. Since, there are two adjacent Cl planes, they are marked as $Cl_1$ and $Cl_2$. The interplanar separation distance between the plane containing all F ions and that containing all Ba ions ($P_1$) is marked in Fig. 5. Also marked are the interplanar distance between Ba and $Cl_1$ planes ($P_2$) and that between $Cl_1$ and $Cl_2$ planes ($P_3$). Fig. 6 shows the temperature dependence of $P_1$, $P_2$ and $P_3$ of the present data (solid line). The error in $P_1$, $P_2$ and $P_3$ are 0.3, 2 and 2%, respectively. The straight lines are guide to

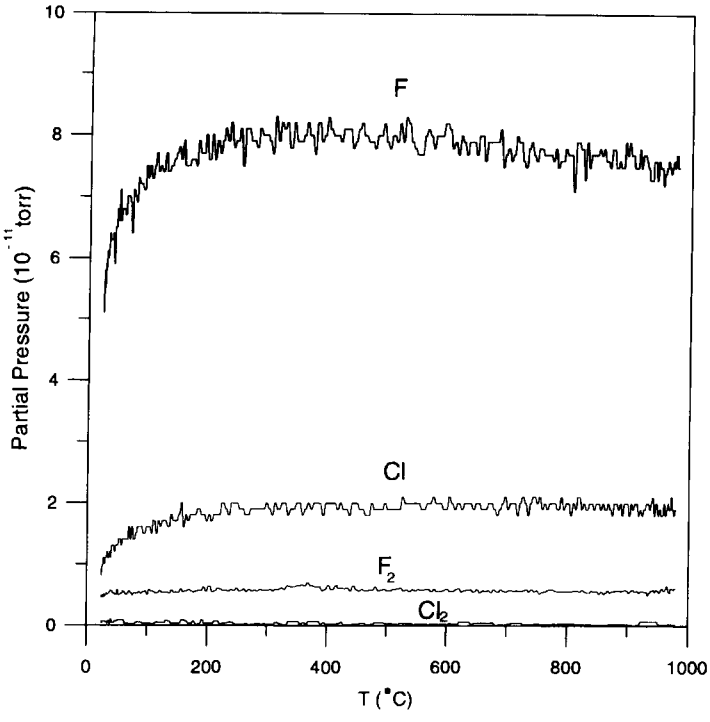


Fig. 4. Evolved gas curves of F, $F_2$, Cl and $Cl_2$.

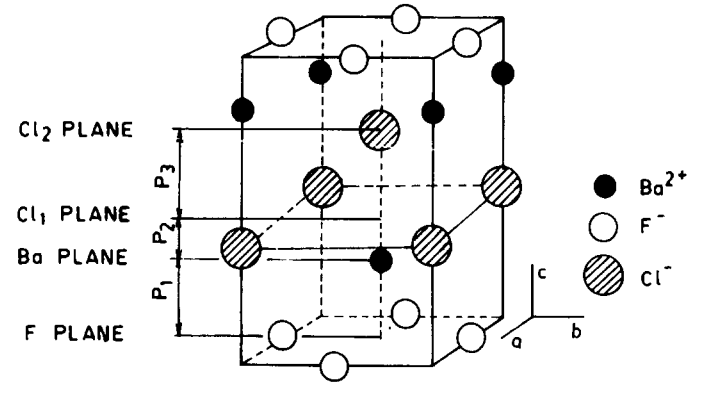


Fig. 5. The unit cell of BaFCl. Various planes and interplanar distances are marked.

the eye. It is interesting to note that the Ba plane moves closer to the F plane but away from $Cl_1$ plane and the $Cl_2$ plane moves away from the $Cl_1$ plane as $T$ increases. When $T$ increases, F vacancies are created more in number than Cl vacancies as shown in Fig. 4 and also the cell expands. Ba relaxes by moving towards the F plane which contains a lot of vacancies. Hence, $P_1$ decreases with increasing temperature. Due to cell expansion, $P_2$ and $P_3$ increase. It would be worth comparing the temperature behaviour of inter-

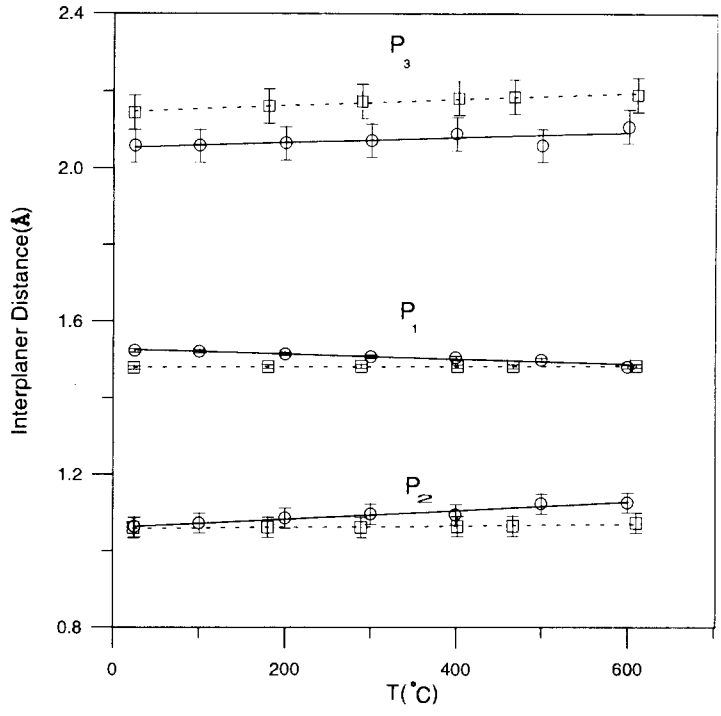


Fig. 6. The temperature dependence of the interplanar separation distances in BaFCl both, the present data and data taken from Kodama et al. [17]. $P_1$, $P_2$, $P_3$ are represented in Fig. 3. (○) The solid lines are straight line fits to the present data and (□) the dashed lines are the straight line fits to Kodama et al. [17] data.

planar separations in a BaFCl single crystal [17]. Fig. 6 also shows the interplanar separations determined from the data of Kodama et al. [17] (dashed line). The values of $P_1$, $P_2$ and $P_3$ of Kodama et al. [17] differ a little from the present values, but their temperature dependence is similar to present data.

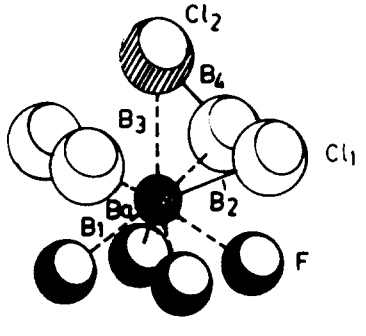


Fig. 7. Coordination polyhedron for the $Cl^-$ and $F^-$ ligands around the central $Ba^{2+}$ in BaFCl. The interionic separation distances are marked.

Fig. 7 illustrates the coordination polyhedron for the Cl and F ion ligands around the central Ba ion in BaFCl. The interionic separation distances between F and Ba ions ($B_1$), between Ba and $Cl_1$ ions ($B_2$), Ba and $Cl_2$ ions ($B_3$), and $Cl_1$ and $Cl_2$ ions ($B_4$) are marked in this figure. Fig. 8 gives the interionic distances ($B_1$, $B_2$, $B_3$ and $B_4$) as a function of temperature for the present (solid lines) and the reported [17] data (dashed lines). The straight lines through the points are guide to eye. $B_1$, $B_2$, $B_3$ and $B_4$ increase with temperature as seen in Fig. 8.

The temperature dependence of the asymmetry parameter, sample displacement parameter, Lorentzian admixture parameter and FWHM of the high-intensity XRD peak are given in Fig. 9. The straight lines are guide to the eye. The Lorentzian admixture with Gaussian line shape decreases with increasing $T$. This behaviour is understandable on the basis that the line-shape function tends to be Gaussian due to a manifestation of the central limit theorem [28] as $T$ increases. The sample displacement parameter

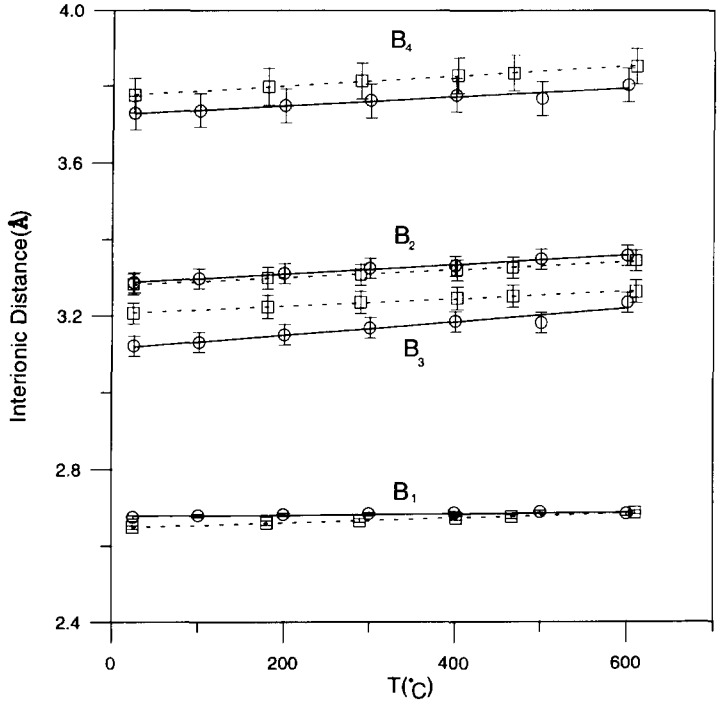


Fig. 8. The temperature dependence of the interionic distances in both, the present data and data taken from Kodama et al. [17]. $B_1$, $B_2$, $B_3$, $B_4$ are marked in Fig. 5. (○) The solid lines are the straight line fits to the present data and (□) the dashed lines are the straight line fits to Kodama et al. [17] data.

decreases continuously with increasing $T$. It is observed that the loosely packed BaFCl powder into the depression in Ta foil sinters at high temperatures. The powder had occupied the full volume of the depression while filling at room temperature but it compacted from all sides at higher temperatures. The sample was a hard pellet-like solid when it was taken out of the foil after the completion of the experiment. The top surface of the sample moved down into the depression as $T$ increases. This surface movement is manifested as the sample displacement in the Rietveld analysis. The linear increase in the asymmetry parameter can also be attributed to sintering. When the sample is loosely packed at room temperature, the XRD signal would be collected over a large thickness of the sample due to a greater penetration of X-ray beam into the loosely packed powder. Since the signal collected from a deeper region of the powder gives an XRD peak slightly shifted down in $2\theta$ value as compared to the signal collected from the surface region of the powder, the resultant XRD peak would have an asymmetric tail on the low $2\theta$ side which is correctly shown in Fig. 9 as negative value for asymmetry parameter. As $T$ increases, the powder sinters, the X-ray beam penetration decreases and, hence, the negative asymmetry tends towards the zero value as depicted in Fig. 9. As $T$ increases further, the asymmetry value increases beyond zero. The reason for this is not clear. The spread of the resultant XRD peak due to the finite X-ray beam penetration into the sample is amply illustrated in the temperature dependence of FWHM of the peak at $2\theta=23.6^\circ$ (Fig. 9). Since the penetration depth decreases with the increase of $T$, the FWHM decreases. The other possible reason for the decrease of FWHM is the increase of the grain size upon sintering which is less likely to occur within a few hours at these temperatures. If the FWHM were to be attributed to the grain size, then the grain size has to increase from 58 nm at room temperature to 80 nm at 600°C which is not very likely.

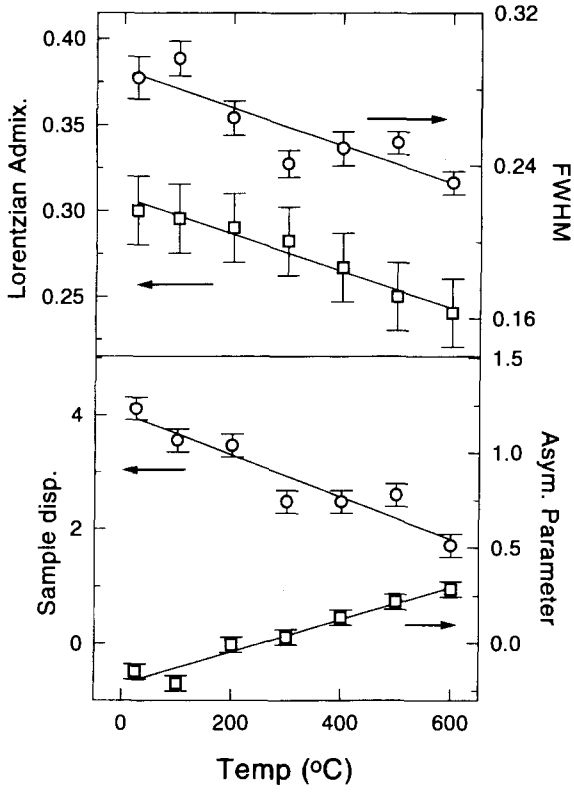


Fig. 9. The temperature dependence of the parameters of the Rietveld analysis: sample displacement, asymmetry of the diffraction peak, Lorentzian admixture of the line shape function and FWHM of the high-intensity diffraction peak. The solid straight lines are guide to the eye.

## Acknowledgements

The authours thank Dr. Kanwar Krishan and Dr. T.S. Radhakrishnan for encouragement, Dr. V. Sridharan for discussions and M. Kamruddin and P.K. Ajikumar for carrying out the EGA experiment.

## References

[1] K. Somaiah, V. Hari Babu, Indian J. Pure and App. Phys. 14 (1976) 702.
[2] Y.R. Shen, T. Gregorian, W.B. Holzapfel, High Press. Res. 7 (1991) 73.
[3] E. Nicklaus, F. Fischer, J. Crystal Growth 12 (1972) 337.
[4] R. Sauvage, Acta Cryst. B 30 (1974) 2786.
[5] K. Takahashi, J. Miyahara, Y. Shibahara, J. Electrochem. Soc. 132 (1985) 1492.
[6] H.L. Bhat, M.R. Srinivasan, S.R. Girisha, A.H. Rama Rao, P.S. Narayanan, Indian J. Pure and App. Phys. 15 (1977) 74.
[7] Y.R. Shen, U. Englisch, L. Chudinovskikh, F. Porsch, R. Haberkorn, H.P. Beck, W.B. Holzapfel, J. Phys.: Condensed Matter 6 (1994) 3197.
[8] J.F. Scott, J. Chem. Phys. 49 (1968) 2766.
[9] D. Nicollin, H. Bill, J. Phys. C: Solid State Phys. 11 (1978) 4803.
[10] B. Sundarakkannan, R. Kesavamoorthy, G.V. Narasimha Rao, in: S. Selvasekarapandian, P. Christober Selvan (Eds.), Luminescence and Its Applications, Allied Publishers Ltd, Madras, 1996, 349.
[11] L. Marculescu, Chem. Phys. Lett. 21 (1978) 342.
[12] K.R. Balasubramanian, T.M. Haridasan, N. Krishnamurthy, Solid State Commun. 32 (1979) 1095.
[13] K.R. Balasubramanian, T.M. Haridasan, J. Phys. Chem. Solids 42 (1981) 667.
[14] K.R. Balasubramanian, T.M. Haridasan, N. Krishnamurthy, Chem. Phys. Lett. 67 (1979) 530.
[15] M. Fischer, M. Sieskind, A. Polian, A. Lahmar, J. Phys.: Condensed Matter 5 (1993) 2749.
[16] P. Herzig, J. Solid State Chem. 57 (1985) 379.
[17] N. Kodama, K. Tanaka, T. Utsunomiya, Y. Hoshino, F. Marumo, Solid State Ionics 14 (1984) 17.
[18] F.K. Koschnick, J.M. Spaeth, R.S. Eachus, J. Phys.: Condensed Matter 4 (1992) 3015.
[19] D. Jumeau, J. Phys. Chem. Solids 37 (1976) 465.
[20] E. Nicklaus, F. Fischer, Phys. Stat. Sol.(b) 52 (1972) 453.
[21] A.S. Krochuk, O.R. Onufrir, Z.P. Chornyi, Phys. Stat. Sol. (b) 154 (1989) K9.
[22] H.M. Rietveld, J. Appl. Cryst. 2 (1969) 65.
[23] D.K. Smith, S. Gorter, J. Appl. Cryst. 24 (1991) 369.
[24] R.A. Young, A. Sakthivel, T.S. Moss, C.O. Paira-Santos, J. Appl. Cryst. 28 (1995) 366.
[25] M. Kamruddin, P.K. Ajikumar, S. Dash, R. Krishnan, A.K. Tyagi, K. Krishan, Thermochim. Acta 287 (1996) 13.
[26] R.S. Krishnan, Thermal Expansion of Crystals, Pergamon Press, Oxford, England, 1976, p. 115.
[27] A. Xenopoulos, M. Ralle, A. Habenschuss, B. Wunderlich, Powder Diff. 11 (1996) 246.
[28] S.S. Willes, Mathematical Statistics, John Wiley and Sons Inc., New York, 1962, 257.